Sedimentary Geology 226 (2010) 42–53

Contents lists available at ScienceDirect

Sedimentary Geology

journal homepage: www.elsevier.com/locate/sedgeo

# Fabric anisotropy induced by primary depositional variations in the silt: clay ratio in two fine-grained slope fan complexes: Texas Gulf Coast and northern North Sea

Ruarri J. Day-Stirrat [a,*], Shirley P. Dutton [a], Kitty L. Milliken [a], Robert G. Loucks [a], Andrew C. Aplin [b], Stephen Hillier [c], Ben A. van der Pluijm [d]

[a] Bureau of Economic Geology, John A. and Katherine G. Jackson School of Geosciences, The University of Texas at Austin, University Station, Box X , Austin, TX, 78713, USA
[b] School of Civil Engineering and Geosciences and Institute for Research in Environment and Sustainability, Devonshire Building, Newcastle University, Newcastle upon Tyne, NE1 7RU, UK
[c] Macaulay Institute, Craigiebuckler, Aberdeen, AB15 8QH, UK
[d] Department of Geological Sciences, University of Michigan, C.C. Little Building, 425 E. University Ave., Ann Arbor, MI 48109-1063, USA

ARTICLE INFO

*Article history:*
Received 6 March 2009
Received in revised form 3 November 2009
Accepted 18 February 2010
Available online 3 March 2010

Communicated by G.J. Weltje

*Keywords:*
Mudstone
Phyllosilicate
Fabric
Textural goniometry
Diagenesis
Anisotropy

ABSTRACT

High-resolution X-ray texture goniometry (HRXTG) has been used to quantify the alignment (anisotropy) of phyllosilicate minerals in a series of diagenetically altered mudstone samples from the deep subsurface of the Texas Gulf Coast and the northern North Sea. The sampled formations have undergone a simple burial history with no overprint of tectonic deformation that may have influenced the phyllosilicate orientation. Observations have been made in two constrained temperature windows 148–150 °C (North Sea data) and 169–210 °C (Texas Gulf Coast) wherein less than 20% smectite remains in the mixed layer phase illite–smectite. Quantitative X-ray powder diffraction (XRPD) shows quartz (which is dominantly detrital) and phyllosilicate content having an inverse relationship. Quantified illite–smectite fabric intensity (phyllosilicate alignments) ranges from low alignment values of 2.42 m.r.d. (multiples of a random distribution) to high alignment values 6.75 m.r.d. and chlorite + kaolinite ranges from 1.80 to 6.46 m.r.d. We propose that the broad range of phyllosilicate fabric intensity observed reflects the range of quartz/phyllosilicate ratios that are the imprint of depositional setting, bedform truncation, and initial grain size. Detrital quartz acts to disrupt fabric intensity by being non-platy, producing areas sheltered from effective stress ('pressure shadows'), and acting as a matrix support. There is no evidence that bioturbation is a significant control on phyllosilicate alignment in these quartz/phyllosilicate mixtures. These findings have important implications for the role of grain-scale alignment on seismic anisotropy in mudstone systems. Fabric intensity in post-diagenetic samples can be predicted from (1) quartz content and (2) total clay content where:

$$y = -7.4x + 64.8 \quad (1)$$

$x$ is fabric intensity (in m.r.d.) and $y$ is total (wt.%) quartz

$$a = 4.2b + 33.7 \quad (2)$$

and $a$ is total (wt.%) clay content and b is fabric intensity (in m.r.d.).



## 1. Introduction

There is an increasing interest in the anisotropy of mudstone systems (Banik, 1984; Ibanez et al., 1992; Vernik and Landis, 1996; Clennell et al., 1999; Sayers, 1999; Johansen et al., 2002; Angabini, 2003; Johansen et al., 2004; Kwon et al., 2004; Sayers, 2005; Dewhurst and Siggins, 2006; Schon et al., 2006; Valcke et al., 2006; Clavaud et al., 2008) driven in part by the effects of grain-scale alignment on seismic anisotropy (Johansen et al., 2004) that is caused by the change in wave velocity and polarization with propagation direction (Valcke et al., 2006). Compressional and shear wave velocities have been noted to change by as much as 20% with an increase in preferred orientation of phyllosilicates (Johnston and Christensen, 1995) creating a seismic anisotropy at depth. At the depositional surface, sediments are predominantly isotropic with little preferred orientation of particles. Changes in seismic anisotropy result in depth conversion errors obtained from surface seismic datasets and imaging problems (Dewhurst and Siggins, 2006) leading to the possible misinterpretation of 'shale tectonics' (see Van Rensbergen and Morley, 2003 for reinterpretation) in the deep subsurface. Further,

* Corresponding author. Tel.: +1 512 471 7313.
*E-mail address:* Ruarri.Day-Stirrat@beg.utexas.edu (R.J. Day-Stirrat).

0037-0738/$ – see front matter © 2010 Elsevier B.V. All rights reserved.
doi:10.1016/j.sedgeo.2010.02.007

anisotropy of phyllosilicates will set up vertical versus horizontal permeability heterogeneities (Kwon et al., 2004) that are probably governed by the relationship of pores and pore throats to phyllosilicate platelets.

Studies by Ho et al. (1999), Worden et al. (2005), Aplin et al. (2006) and Day-Stirrat et al. (2008) discuss the control of illitization of smectite on the fabric intensity (preferred alignment) of phyllosilicates in the deep subsurface and have moved the debate surrounding the mechanisms for imparting a phyllosilicate anisotropy beyond a simple mechanical compaction model (Oertel and Curtis, 1972; Curtis et al., 1980; Sintubin, 1994). Implicit in a diagenetic model for an increase in phyllosilicate anisotropy is a mechanism for the illitization of smectite (Burst, 1959; Hower and Mowatt, 1966; Powers, 1967; Hower et al., 1976; Boles and Franks, 1979) that calls for dissolution of a precursor phase and recrystallization into a neo-formed phase (Boles and Franks, 1979) or at least partial dissolution (Ahn and Peacor, 1986; Inoue et al., 1987) in a high effective stress regime in which the 'platy' neo-formed phyllosilicates grow perpendicular to maximum effective stress. It is also implicit based on the work of O'Brien (1970, 1971), O'Brien and Slatt (1990), Bennett et al. (1991), and Kranck et al. (1996) that initial depositional phyllosilicate assemblages are isotropic.

In this study high-resolution X-ray texture goniometry (HRXTG) (van der Pluijm et al., 1994), X-ray powder diffraction (XRPD) and imaging techniques are employed to quantify and visualize the alignment of phyllosilicates in a series of deeply buried mudstones deposited in two lowstand systems tract settings. Samples have been buried to 6.6 and 4.8 km and temperatures of 210 °C and 150 °C in the Texas Gulf Coast and Northern North Sea, respectively. The sampled mudstones are diagenetically mature with porosity highly reduced, greater than 50 Ma old and have a relatively simple burial history.

The dataset systematically examines mudstones and siltstones for the influence of quartz/phyllosilicate ratio as a control on phyllosilicate anisotropy beyond the illitization of smectite under conditions of high effective stress. We present a conceptual model to describe this in terms of grain dimension, diagenesis and effective stress distribution and present equations to predict fabric intensity as a function of composition.

## 2. Samples and geological setting

### 2.1. ARCO #1 W. L. Crews, Gulf Coast

Eocene Lower Wilcox Formation samples (5793–6613 m) and Eocene Yegua Formation samples (4966–4972 m) from the ARCO #1 W. L. Crews well from Brazoria County, Texas (Fig. 1) were selected for analysis (Dutton and Loucks, 2008). Core sections display upwards-fining fine-grained sandstones inter-layered with mudstones in a slope fan complex (Dutton and Loucks, 2010). Mudstone core plugs were taken for X-ray powder diffraction and high-resolution X-ray texture goniometry analysis as well as optical microscopy, back-scattered electron microscopy and X-ray mapping. Slabbed cores display Bouma sequences (Bouma, 1962) on the scale of millimeters and have upwards-fining sequences in hand specimen and some evidence for depositional slump structures. The samples are hard and non-fissile.

The Wilcox Formation of the late Paleocene–early Eocene represents the first major regional siliciclastic wedge built over and beyond the Cretaceous carbonate shelf along the Texas Gulf Coast (Fisher and McGowen, 1967; Galloway et al., 2000). In Texas, the Lower Wilcox Formation produces hydrocarbons along a strip paralleling the coastline from the Louisiana to the Mexican border and an outcrop distribution paralleling this further inland. Wilcox Formation thicknesses range from ~300 m in outcrop to more than 3000 m in the deep subsurface under the current position of the Gulf of Mexico coastline. Siliciclastic deposition occurred on a broad, flat, low-lying coastal plain with drainage axes approximately comparable to the modern day drainage pattern (Galloway and McGilvery, 1995; Galloway et al., 2000; Galloway, 2005 and references therein).

### 2.2. Rhum Field, North Sea

The Late Jurassic Kimmeridge Clay Formation from the Rhum 3/29a4 well in the Rhum Field (Rhum in Fig. 2) has a present day burial depth of 4707–4830 m. Interbedded mudstone and siltstone horizons are present in reservoir sandstone units. Siltstones from a deep-marine, submarine-fan and slope apron complex grade up into well lithified, dark grey to brownish black mudstones which have some fissility and are well-laminated.

The detailed analysis of onshore and offshore areas has demonstrated that marine mudstones were both numerous and distinctive throughout the Late Jurassic of the North Sea. Very slow sedimentation rates associated with mudstone and siltstone deposition promoted the growth of authigenic minerals (e.g. pyrite) (MacQuaker et al., 1997) and preserved high amounts of total organic carbon in the Upper Jurassic Kimmeridge Clay which is the source rock for the major hydrocarbon plays of the North Sea (Glennie, 1998).

### 2.3. Maximum burial temperature

Corrected bottom hole temperatures using a time since circulation method (Corrigan, 2003) were used as input parameters, along with

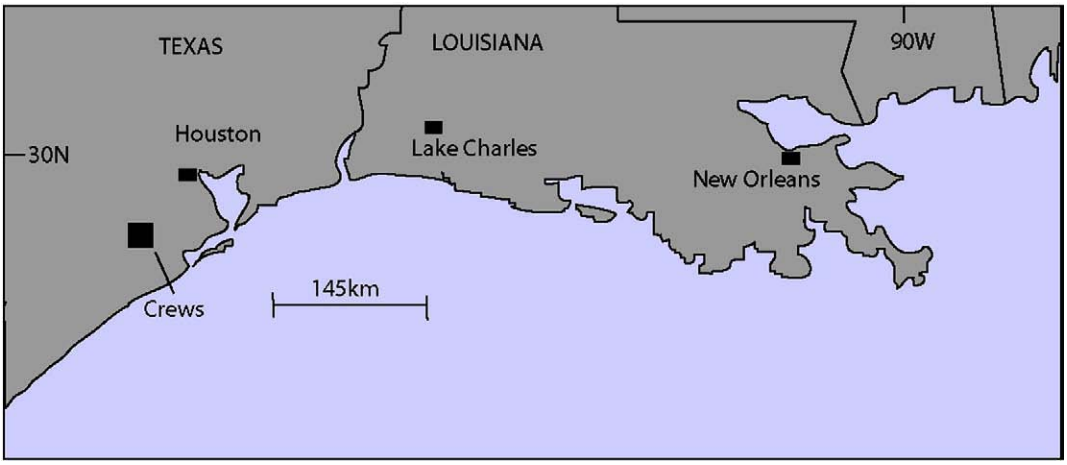


**Fig. 1.** Location of the ARCO #1 W. L. Crews well, Brazoria County, Texas.

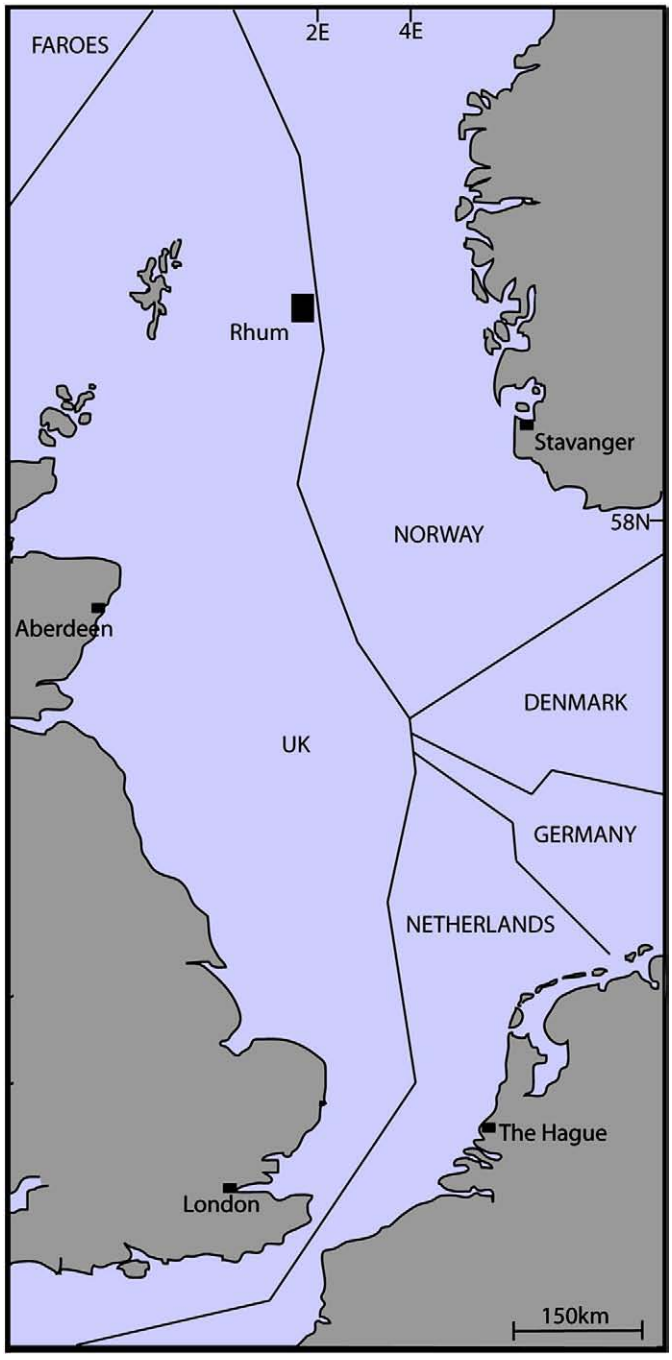


**Fig. 2.** Location of the Rhum 3/29 block in the Northern North Sea.

porosity and vitrinite reflectance, for 1-D thermal models that were utilized to gain temperature data points for each sample depth. Modeling suggests rapid burial from the Eocene to the present for the Crews well. Rhum, by contrast, is characterized by slow burial from the Jurassic to the Eocene but a rapid burial profile in the Miocene–Pliocene associated with the graben formation of the North Sea. No significant hiatuses in deposition or unconformities related to erosion are interpreted from completion logs. The burial history model describes Jurassic samples from the Rhum well that have been subject to temperatures above 150 °C. The base of the Crews well is currently at 210 °C at 6.6 km (21,700 ft) with an associated geothermal gradient of 31.8 °C/km. Deposition began at 53.6 Ma accumulating 6.6 km of sediment without significant erosion events at a rate of 123 m/Ma. The Jurassic of Rhum is at a temperature of 148 °C at 4.8 km (30.8 °C/km), and the sedimentation rate is calculated to be 30 m/Ma. Both wells are significantly overpressured. The Crews well has a pressure of ~95 MPa in the Wilcox Formation, which equates to an excess pressure of ~30 MPa. Rhum has similar excess pressures with current fluid pressures of ~80 MPa in the Jurassic horizons.

## 3. Methods

### 3.1. X-ray powder diffraction (XRPD)

Mineralogical analyses by X-ray powder diffraction (XRPD) methods were made of the whole rock bulk samples and of <2 μm clay-sized fractions, obtained by gentle crushing, disaggregation, dispersion and timed sedimentation. For the whole rock analysis samples were prepared by McCrone milling of 3 g of sample in water, followed by spray drying of the resulting slurry to obtain random powder specimens, as described by Hillier (1999; 2002). Clay-sized fractions were prepared by mounting the clay onto glass slides by a filter peel transfer method to obtain highly oriented specimens (Moore and Reynolds, 1997; Hillier, 2003). All XRPD patterns were recorded on a Siemens D5000 X-ray diffractometer, using Cu Kα radiation, selected by a diffracted beam graphite monochromator. Whole rock samples were scanned from 2–75 ° 2θ, counting for 2 s per 0.02 ° step. Clay fractions were scanned, from 2–45 ° 2θ, counting for 1 s per 0.02 ° step, in the air-dried state, following glycolation by a vapour pressure method overnight, and following heating to 350 °C for 1 h. Quantitative mineralogical analysis of the whole rock data were made by a full pattern fitting, normalized reference intensity ratio method, as described in Omotoso et al. (2006 p.18). Detailed identification of clay minerals in the clay-sized fraction was made by procedures given in Moore and Reynolds (1997) and Hillier (2003).

### 3.2. High-resolution X-ray texture goniometry

A quantitative assessment of the alignment of phyllosilicates was made on an Enraf-Nonius CAD4 automated single-crystal diffractometer using the High-resolution X-ray Texture Goniometry (HRXTG) method described by van der Pluijm et al. (1994). First, samples were scanned over the range of 0.5–6.0 ° º2θ Mo (1–13 ° º2θ Cu), in order to determine which clay mineral phases were present and the exact diffraction angles at which textural data should be collected. The second step of the measurement process involved the "pole-figure scan" (Ho et al., 1995), in which the degree of preferred orientation of previously identified phyllosilicates is determined. The goniometer and detector are fixed at the diffraction angle corresponding to the d-spacing of the 001 or 002 reflection of the chosen phase (identified over the 0.5–6.0 ° º2θ Mo scan). Thin-sections of the sample, 200–500 μm thick cut perpendicular to bedding, were then rotated around two axes, one parallel to an imaginary line connecting the goniometer and detector (designated as φ), and one normal to it (designated as ω). Diffracted X-ray intensity data are collected every 2.5 ° between 0–360 ° around the φ axis, and in nine steps between 0–40 ° around the ω-axis. In total, 1296 intensity measurements are thus made on each sample and are corrected for sample absorption, grain density and specimen thickness (van der Pluijm et al., 1994).

The degree of alignment is obtained from the intensity distribution of diffracted X-rays. Intensity data are displayed in pole figure diagrams that show the distribution of crystallographic orientations in the form of poles to crystallographic planes. Pole figure diagrams visualize the spatial distribution of the X-ray intensities by displaying contour lines representing the pole distribution of phyllosilicate 001 plane orientations. More highly aligned fabrics yield pole figures that can be contoured as concentric rings; completely random or isotropic fabrics yield figures that have no poles. The degree of particle alignment is expressed as maximum pole densities in multiples of a random distribution [m.r.d.] (Wenk, 1985), where higher values

**Table 1**
Results (wt.%) of quantitative analysis of the whole rock samples by the RIR method for samples from the ARCO #1 W. L. Crews well.

| Sample | Depth (m) | Quartz | Plagioclase | K-spar | Calcite | Dolomite/ankerite | Siderite | Pyrite | Jarosite |
|---|---|---|---|---|---|---|---|---|---|
| Crews 4a | 4970 | 37.8 | 7.2 | 1.1 | 0.8 | 0.0 | 0.6 | 0.7 | 2.2 |
| Crews 08 | 5793 | 16.4 | 11.1 | 0.6 | 0.1 | 1.1 | 0.4 | 0.8 | 0.2 |
| Crews 11 | 5795 | 38.9 | 14.6 | 1.2 | 0.0 | 1.3 | 0.4 | 0.6 | 0.0 |
| Crews 14 | 5798 | 29.7 | 10.0 | 0.6 | 0.0 | 1.6 | 3.4 | 1.0 | 0.1 |
| Crews 20 | 5808 | 35.8 | 11.0 | 0.3 | 0.0 | 2.5 | 0.4 | 0.9 | 0.0 |
| Crews 22 | 5813 | 39.4 | 8.4 | 0.6 | 0.0 | 0.0 | 1.0 | 0.2 | 0.2 |
| Crews 33 | 6603 | 36.8 | 5.4 | 0.7 | 0.0 | 0.2 | 0.2 | 0.2 | 0.0 |
| Crews 38 | 6813 | 42.8 | 6.2 | 0.4 | 0.1 | 0.6 | 2.7 | 0.4 | 0.1 |

| Sample | Depth (m) | Anatase | Mica 2M1 | Illite | I–S | Kaolinite | Chlorite | Totals | Total clay |
|---|---|---|---|---|---|---|---|---|---|
| Crews 4a | 4970 | 0.9 | 4.1 | 10.1 | 26.3 | 6.9 | 1.3 | 100.0 | 48.7 |
| Crews 08 | 5793 | 0.6 | 13.4 | 11.3 | 32.0 | 4.5 | 7.5 | 100.0 | 68.7 |
| Crews 11 | 5795 | 0.6 | 7.8 | 11.3 | 15.5 | 0.9 | 6.8 | 99.9 | 42.3 |
| Crews 14 | 5798 | 0.4 | 10.0 | 12.1 | 21.7 | 0.1 | 9.2 | 99.9 | 53.1 |
| Crews 20 | 5808 | 0.8 | 10.6 | 5.3 | 26.2 | 0.0 | 6.3 | 100.1 | 48.4 |
| Crews 22 | 5813 | 0.3 | 5.3 | 11.4 | 30.4 | 0.6 | 2.1 | 99.9 | 49.8 |
| Crews 33 | 6603 | 0.7 | 6.4 | 16.9 | 29.3 | 0.3 | 2.9 | 100.0 | 55.8 |
| Crews 38 | 6813 | 0.5 | 4.8 | 11.9 | 25.3 | 0.0 | 4.1 | 99.9 | 46.1 |

**Table 2**
Results (wt.%) of quantitative analysis of the whole rock samples by the RIR method for samples from Rhum 3/29a4.

| Sample | Depth (m) | Quartz | Plagioclase | K-spar | Calcite | Dolomite/Ankerite | Siderite | Pyrite | Jarosite |
|---|---|---|---|---|---|---|---|---|---|
| Rhum | 4707 | 82.9 | 1.1 | 0.0 | 0.1 | 0.4 | 0.2 | 3.7 | 0.1 |
| Rhum | 4759 | 35.1 | 2.0 | 0.0 | 0.0 | 0.5 | 0.0 | 7.6 | 0.0 |
| Rhum | 4771 | 36.9 | 0.3 | 0.6 | 0.1 | 0.0 | 0.0 | 8.0 | 0.7 |
| Rhum | 4830 | 23.3 | 0.3 | 1.2 | 0.6 | 1.1 | 0.8 | 11.6 | 2.0 |

| Sample | Depth (m) | Anatase | Mica 2M1 | Illite | I–S | Kaolinite | Chlorite | Totals | Total clay |
|---|---|---|---|---|---|---|---|---|---|
| Rhum | 4707 | 0.0 | 1.6 | 3.3 | 4.8 | 1.7 | 0.0 | 99.9 | 11.4 |
| Rhum | 4759 | 0.5 | 3.3 | 12.3 | 23.3 | 15.4 | 0.0 | 100.0 | 54.3 |
| Rhum | 4771 | 0.6 | 6.1 | 17.3 | 19.6 | 9.9 | 0.0 | 100.1 | 52.9 |
| Rhum | 4830 | 0.8 | 9.3 | 13.0 | 33.8 | 2.2 | 0.0 | 100.0 | 58.3 |

reflect higher degrees of alignment. Intensity is dependent on the concentration of crystals aligned parallel to each other. A value for the multiples of a random distribution is produced even when the sample has not been prepared perpendicular to bedding, so a stereographic projection showing centered contour lines validates the multiples of a random distribution value.

### 3.3. Mercury porosimetry

Porosity and pore throat size distributions were determined on a one gram block of sample that was freeze dried (Delage and Lefebvre, 1984) for 24 h, then dried in an oven at 105 °C for a further 24 h. Porosities were calculated from bulk volume and grain density. Analysis took place on a *Micromeritics*© Autopore Π 9220 machine and yielded a figure for porosity, and a pore throat size distribution. Pore throat diameters were calculated from the mercury intrusion data. The analysis used the assumption that the surface tension of mercury was 0.48 N/m and the contact angle between mercury and the particle surface was 141 °. The pore throat radius, r, is given by:

$$r = 746{,}000/_{p}$$

where $r$ is the pore throat radius (nm) and $p$ is the pressure in kPa.

**Table 3**
Relative percentages of clay minerals in the <2 μm clay size fraction from the ARCO #1 W. L. Crews well.

| Sample | Depth (m) | Chlorite | Kaolinite | Illite | Illite–smectite | % exp* |
|---|---|---|---|---|---|---|
| Crews 4a | 4970 | | 6 | 7 | 87 | 20 |
| Crews 08 | 5793 | 7 | 2 | 18 | 73 | 15 |
| Crews 11 | 5795 | 7 | 2 | 18 | 73 | 15 |
| Crews 14 | 5798 | 10 | | 20 | 70 | 20 |
| Crews 20 | 5808 | 7 | | 18 | 75 | 20 |
| Crews 22 | 5813 | 2 | | 8 | 90 | 20 |
| Crews 33 | 6603 | 2 | | 13 | 85 | 15 |
| Crews 38 | 6813 | 3 | | 11 | 86 | 15 |

### 3.4. Thin-sections and optical microscopy

Thin-section scans were imaged on a Konica Minolta DiMAGE scan elite 5400. Images were manually focused and were unprocessed by the DiMAGE software. Optical microscopy was performed on a standard petrographic microscope and images were captured with a digital camera. Due to sample thicknesses and the fine-grained nature of the samples only images at 2.5× magnification were saved.

### 3.5. Backscattered Electron Microscopy and X-ray mapping

The thin-sections for the backscattered electron microscopy (BSE) observations were prepared perpendicular to bedding with a surface oriented parallel to that of the section for HRXTG, allowing direct comparison. The BSE thin-section was polished to a microprobe finish

**Table 4**
Relative percentages of clay minerals in the <2 μm clay size fraction from Rhum 3/29a4.

| Sample | Depth (m) | Kaolinite | I+I–S | % exp* |
|---|---|---|---|---|
| Rhum | 4707 | 13 | 87 | ≤10 |
| Rhum | 4759 | 22 | 78 | ≤10 |
| Rhum | 4771 | 10 | 90 | ≤10 |
| Rhum | 4830 | | 100 | ≤10 |

using repeated vacuum surface impregnations. We used a JEOL 8200 Microprobe equipped with an energy dispersive X-ray detector (EDS), and a back-scattered electron detector. The machine was operated at 15 kV and 30 nA, with a spot size of 1 μm and a working distance of around 11 mm in back-scattered mode. X-ray maps were collected for sodium, magnesium, iron and potassium. A focused 1 μm spot with a 15 kV accelerating voltage and a 30 nAmp current on brass was used. Elements were mapped with wavelength dispersive spectra over a 1024×1024 pixel grid, with 1 pixel equating to 1 μm. The X-ray maps are rendered as false color images and consistent levels were used from sample to sample so qualitative assessments of abundance could be made.

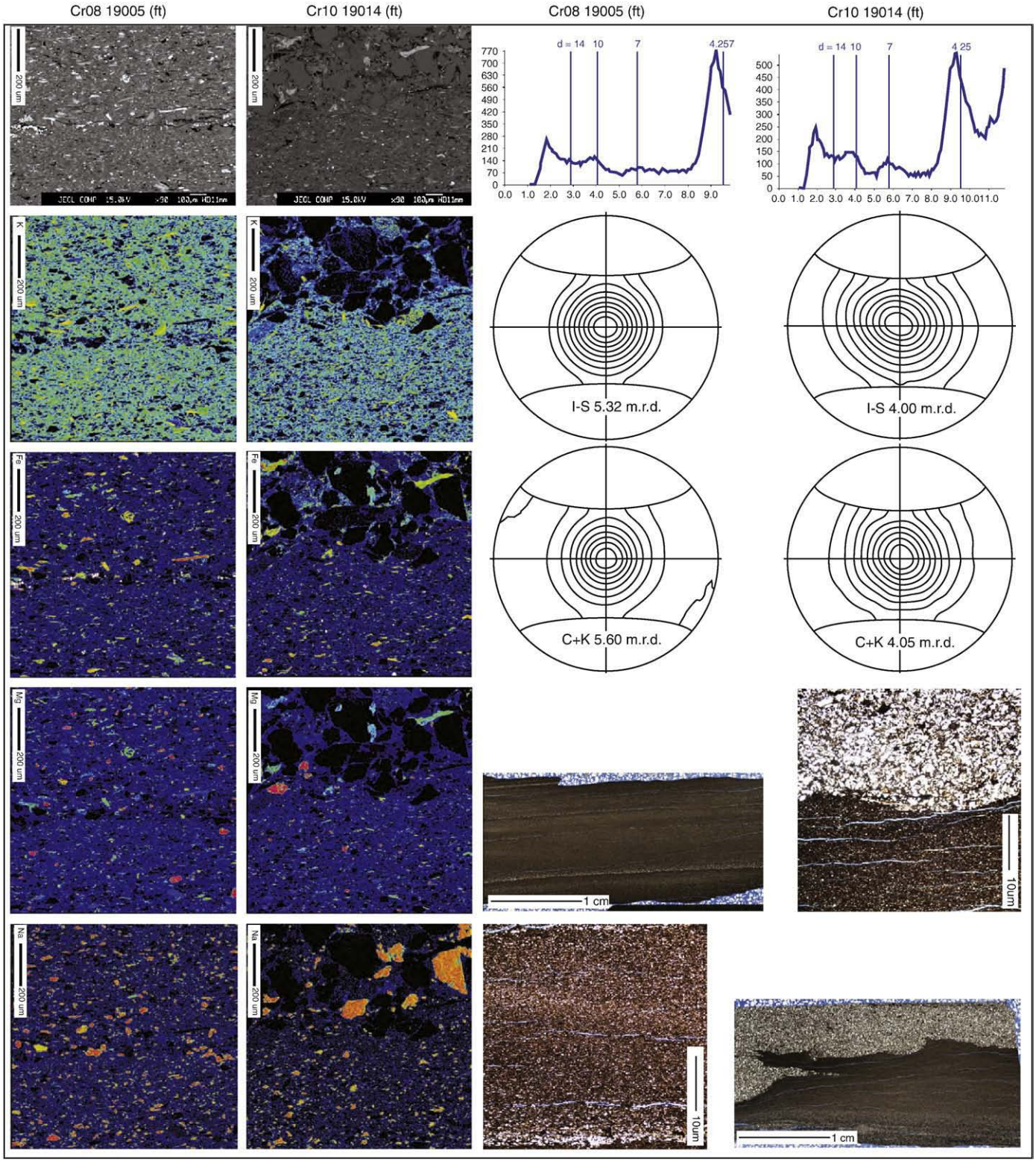


**Fig. 3.** BSE images and associated X-ray maps for potassium, iron, magnesium and sodium for samples Cr08 (5793 m) and Cr10 (5795 m). 2-theta scans and full pole figures with alignment quoted as m.r.d. for samples for samples Cr08 and Cr10 and thin-section photographs and optical microscope images.

**Table 5**
HRXTG data. Maximum intensity in m.r.d. for the illite–smectite and chlorite + kaolinite peaks, 2-theta position for illite–smectite and chlorite + kaolinite, calculated d-spacing for illite–smectite and chlorite + kaolinite and time since circulation bottom hole temperature for Rhum 3/29a4.

| Sample ID | Depth (m) | Max. pole density m.r.d 'I–S' | Max. pole density m.r.d 'C–K' | 2-theta 'I–S' | 2-theta 'C–K' | Kα ave. d-spacing 'I–S' | Kα ave. d-spacing 'C–K' | Temp [C] | Formation |
|---|---|---|---|---|---|---|---|---|---|
| R4707 | 4707 | 5.82 | 2.92 | 3.83 | 5.77 | 10.43 | 6.86 | 148 | KCF |
| R4712 | 4712 | 6.11 | 4.06 | 3.89 | 5.64 | 10.27 | 7.02 | 148 | KCF |
| R4712r | 4712 | 6.08 | 3.99 | 3.92 | 5.75 | 10.19 | 6.89 | 148 | KCF |
| R4759 | 4759 | 4.85 | 4.32 | 3.73 | 5.74 | 10.8 | 6.98 | 148 | KCF |
| R4771 | 4771 | 6.05 | 5.19 | 3.76 | 5.64 | 10.18 | 7.07 | 149 | KCF |
| R4771r | 4771 | 5.52 | 4.4 | 3.88 | 5.56 | 10.34 | 7.17 | 149 | KCF |
| R4830 | 4830 | 6.27 | 2.07 | 3.95 | 5.52 | 10.06 | 7.13 | 150 | KCF |
| R4830x | 4830 | 4.26 | 1.8 | 3.64 | 5.58 | 10.99 | 7.1 | 150 | KCF |

## 4. Results

### 4.1. X-ray powder diffraction (XRPD)

Quartz is relatively abundant in most mudstone samples from the Crews well (Table 1). Plagioclase is the dominant feldspar but minor quantities of K-feldspar (<1.1 wt.%) are detected. However, the large uncertainty on K-feldspar contents at these levels suggests that it may not be present at all in some samples. K-feldspar limit of detection is estimated at 0.5–0.7 wt.% at 95% confidence in the measured patterns by the RIR method (Hillier, 2003). The carbonates, along with pyrite, anatase and jarosite, are detected in minor amounts, with jarosite presumably related to pyrite oxidation post-sampling. Of the clay minerals mixed-layer illite–smectite (I–S) is the most abundant component, accounting for ~30 wt.% of the rock in most cases. Illite accounts for ~11 wt.%, kaolinite is rare except for two exceptions. Many of the samples contain a further 2:1 clay, chlorite that comprises up to 9.2 wt.%.

The whole rock analyses of the Rhum samples (Table 2.) show that the main minerals are quartz, the clay minerals illite–smectite, illite and kaolinite (chlorite is absent) and large amounts of pyrite. The large quartz content of the sample from 4707 m suggests that the overlying reservoir sandstone was sampled accidentally. The total clay is ~5 wt.% higher than the Crews well. Traces of carbonates, as well as anatase and jarosite are also variably detected. The feldspars (plagioclase and K-feldspar) total no more than 2.0 wt.%.

Analyses of the <2 μm clay fraction of the Crews and the Rhum samples are presented in Tables 3 and 4, respectively. Samples from the Crews well are dominated by mixed-layer illite–smectite with expandability ranging from 20–15%. The shallowest samples show some evidence of R1 ordering (Jadgozinski, 1949) in illite–smectite. Minor illite is a ubiquitous component and minor to trace amounts of kaolinite are detected in the shallowest three samples. Chlorite is present in all the Wilcox Formation samples and accounts for 2–10% of all clays. The <2 μm clay fraction of the Rhum samples is dominated by a mixture of illite and mixed-layer illite–smectite with minor to moderate kaolinite in 3 of 4 samples. The mixed-layer illite–smectite is of low expandability, such that illite cannot be readily quantified separately from illite–smectite and the two instead are combined. Three of the four clay fractions were contaminated by quartz which often indicates that a fine component of quartz exists in the rock. Chlorite is below the limit of detection.

### 4.2. High-resolution X-ray texture goniometry

Representative 2-theta scans and pole figures for the preferred orientation of phyllosilicates are presented in Fig. 3. Two phyllosilicate peaks for each sample from the Crews and Rhum wells were selected for alignment analysis. The maximum peak close to a d-spacing of 10 Å corresponding to 001 peak of illite or illite/smectite (see Tables 5 and 6 for exact positions) was analyzed along with the peak at a d-spacing of 7 Å (002 of chlorite/001 of kaolinite). The pole figures show well centered poles with only minor data lost to the unmeasured area (van der Pluijm et al., 1994; Sintubin, 1995; van der Pluijm et al., 1995). There is a strong relationship between the illite/smectite and chlorite + kaolinite peak in

**Table 6**
HRXTG data. Maximum intensity in m.r.d. for the illite–smectite and chlorite + kaolinite peaks, 2-theta position for illite–smectite and chlorite + kaolinite, calculated d-spacing for illite–smectite and chlorite + kaolinite and time since circulation bottom hole temperature for ARCO # W. L. Crews.

| Sample ID | Depth (m) | Max. intensity m.r.d 'I–S' | Max. intensity m.r.d 'C–K' | 2-theta 'I–S' | 2-theta 'C–K' | Kα ave. d-spacing 'I–S' | Kα ave. d spacing 'C–K' | Temp [C] | Formation |
|---|---|---|---|---|---|---|---|---|---|
| C0r2 | 4966 | 6.75 | 6.46 | 3.86 | 5.68 | 10.56 | 7.18 | 169 | Yegua |
| Cr02X | 4966 | 5.96 | 6.07 | 4.05 | 5.80 | 10.06 | 7.03 | 169 | Yegua |
| Cr03 | 4967 | 4.73 | 5.33 | 4.01 | 5.80 | 10.16 | 7.03 | 169 | Yegua |
| Cr04a | 4970 | 3.93 | 3.75 | 3.86 | 5.68 | 10.56 | 7.18 | 169 | Yegua |
| Cr07 | 4972 | 4.04 | 4.07 | 3.75 | 5.85 | 10.87 | 6.97 | 169 | Yegua |
| Cr08 | 5793 | 5.32 | 5.60 | 3.96 | 5.80 | 10.29 | 7.03 | 187 | Wilcox |
| Cr10 | 5795 | 4.00 | 4.05 | 3.90 | 5.74 | 10.45 | 7.11 | 187 | Wilcox |
| Cr14 | 5798 | 4.32 | 4.38 | 3.95 | 5.80 | 10.32 | 7.03 | 187 | Wilcox |
| Cr17 | 5804 | 6.03 | 6.05 | 4.05 | 5.80 | 10.06 | 7.03 | 187 | Wilcox |
| Cr20 | 5808 | 4.23 | 4.24 | 3.94 | 5.80 | 10.34 | 7.03 | 187 | Wilcox |
| Cr21 | 5809 | 3.93 | 3.85 | 3.90 | 5.80 | 10.45 | 7.03 | 187 | Wilcox |
| Cr22 | 5813 | 3.85 | 3.17 | 3.76 | 5.77 | 10.84 | 7.07 | 187 | Wilcox |
| Cr26 | 6374 | 2.76 | 2.22 | 3.86 | 5.80 | 10.56 | 7.03 | 202 | Wilcox |
| Cr28 | 6376 | 2.92 | 2.44 | 3.80 | 5.64 | 10.72 | 7.23 | 202 | Wilcox |
| Cr28X | 6376 | 3.09 | 2.49 | 3.86 | 5.76 | 10.56 | 7.08 | 202 | Wilcox |
| Cr29 | 6378 | 2.42 | 2.11 | 3.65 | 5.80 | 11.16 | 7.03 | 202 | Wilcox |
| Cr29X | 6378 | 2.64 | 2.13 | 3.86 | 5.80 | 10.56 | 7.03 | 202 | Wilcox |
| Cr31 | 6603 | 3.43 | 3.47 | 3.92 | 5.71 | 10.40 | 7.14 | 210 | Wilcox |
| Cr33 | 6603 | 3.36 | 3.50 | 3.90 | 5.80 | 10.45 | 7.03 | 210 | Wilcox |
| Cr35 | 6607 | 1.97 | 1.94 | 4.05 | 5.80 | 10.06 | 7.03 | 210 | Wilcox |
| Cr38 | 6613 | 2.80 | 2.64 | 3.80 | 5.77 | 10.72 | 7.07 | 210 | Wilcox |
| Cr38R | 6613 | 2.76 | 2.94 | 3.86 | 5.80 | 10.56 | 7.03 | 210 | Wilcox |

the Crews well with an $R^2$ value of 0.9552. However, this strong relationship is not seen in the Rhum samples, which have an $R^2$ value of 0.0876 and is related to the lower alignment of chlorite + kaolinite than illite–smectite. The alignment calculated for the illite/smectite peak is comparable between the upper parts of the Crews well and Rhum well. However, Rhum has markedly lower values for the chlorite + kaolinite peak compared to the Wilcox Formation of the Crews well.

### 4.3. Thin-sections and optical mineralogy

Thin-sections cut perpendicular to bedding can be seen in Fig. 3 and optical microscopy images are presented in Fig. 5. Thin-sections are parallel to HRXTG subsample. On the scale of 0.5 cm sample Cr08 (Fig. 3) shows at least three cycles of upwards-fining sequences followed by scour or truncation by coarser quartz-rich sediment. Sample Cr10 has a 1 cm fining upwards sequence, which has a phyllosilicate-rich top and grades up from a silty quartz-rich base, terminated by a coarser sandstone unit. There is also evidence for soft-sediment deformation. In contrast, the sample from Rhum at 4707 m has a much more strongly laminated fabric (Fig. 4). Upwards-fining sequences are not present in all samples; Cr14 shows a more random fabric with little size sorting (Fig. 5).

### 4.4. Backscattered Electron Microscopy and X-ray maps

BSE images are presented in Figs. 3 and 5. They show the range of fabrics and fabric inhibitors found in samples from the Crews and Rhum wells. Upwards-fining sequences are typically defined by a quartz-rich base that truncates the top of the previous fining-upwards sequence. In the Crews well these quartz-rich zones are characterized by chlorite cements and lesser amounts of localized ankerite that produces brighter contrasts in BSE images. Significant phyllosilicate fabric inhibitors are quartz and other equidimensional grains (feldspar and carbonates) as well as pyrite framboids. Pyrite is pervasive in some units, especially the Upper Jurassic of the North Sea. Some other textural features present in the Crews well are Fe-rich rims on dolomite grains and the association of pyrite with organic matter. Sample Cr20 (Fig. 5) has a distinct lack of depositional sorting with equidimensional grains set in a matrix of fine phyllosilicate-rich sediment.

X-ray maps have been produced for sodium, iron, magnesium and potassium (Fig. 3). The potassium maps act as a proxy for the distribution of potassium-bearing clays (illite and mica) in these samples and also K-feldspar. The differentiation between tectosilicates and sheet silicates is based on shape; illite and mica are platy whereas K-feldspar is more equant, but only observed as one grain in one sample (XRPD confirms their low levels). Platy phyllosilicates are oriented roughly perpendicular to maximum effective stress (Fig. 3), with this relationship becoming less defined at the contact with the coarser-grained quartz-rich truncation. The regions of high iron concentration correspond to the distribution of large detrital chlorite grains and some smaller possibly authigenic chlorite along with pyrite. Chlorite distributions in the matrix of the fine-grained fraction are also revealed by the magnesium maps, along with isolated dolomite grains. In the quartz-rich zone the iron is related to ankerite cement, however this cement is only visible between coarse grains in the quartz-rich zone and is not present in the mudstones/ siltstones according to the XRPD data. Sodium in albite shows a decrease in abundance with decreasing grain-size, exemplified by the area under the quartz-rich zone in sample Cr08 where the grain size is at its finest and albite is absent.

### 4.5. Mercury porosimetry

Porosity and mean pore throat size distributions for the Crews well (insufficient sample was available for the Rhum well) can be seen in Table 7. Porosity determined by mercury porosimetry ranges between 6 and 10% and mean pore throat sizes were between 8 and 13 nm. A calculated porosity for the Rhum well from density log is ~5% based on the tuned equation of Okiongbo (2005).

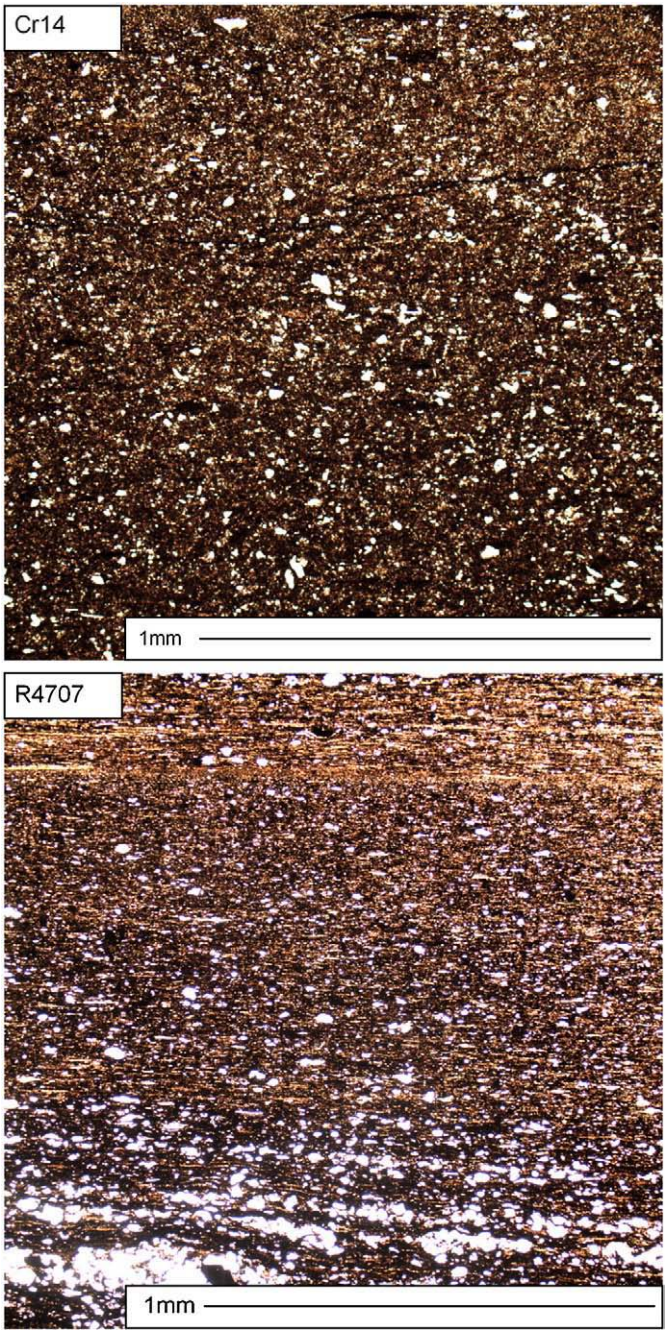


**Fig. 4.** Optical microscopy images of Cr14 (Crews well 19,023 ft/5798 m) and R4707 (Rhum 4707 m). Cr14 has a notable lack of apparent alignment whereas R4707 has an apparent alignment increase from bottom to top of image.

## 5. Discussion

The lowest temperature samples have a present day burial temperature of 150 °C, and this is assumed to also represent the maximum burial temperature based on thermal models. At temperatures greater than 150 °C the extent of most clay-mineral diagenetic reactions is essentially complete (Hoffman and Hower, 1979; Pytte and Reynolds, 1989; Walker, 1993; Hillier et al., 1995) with 75% or

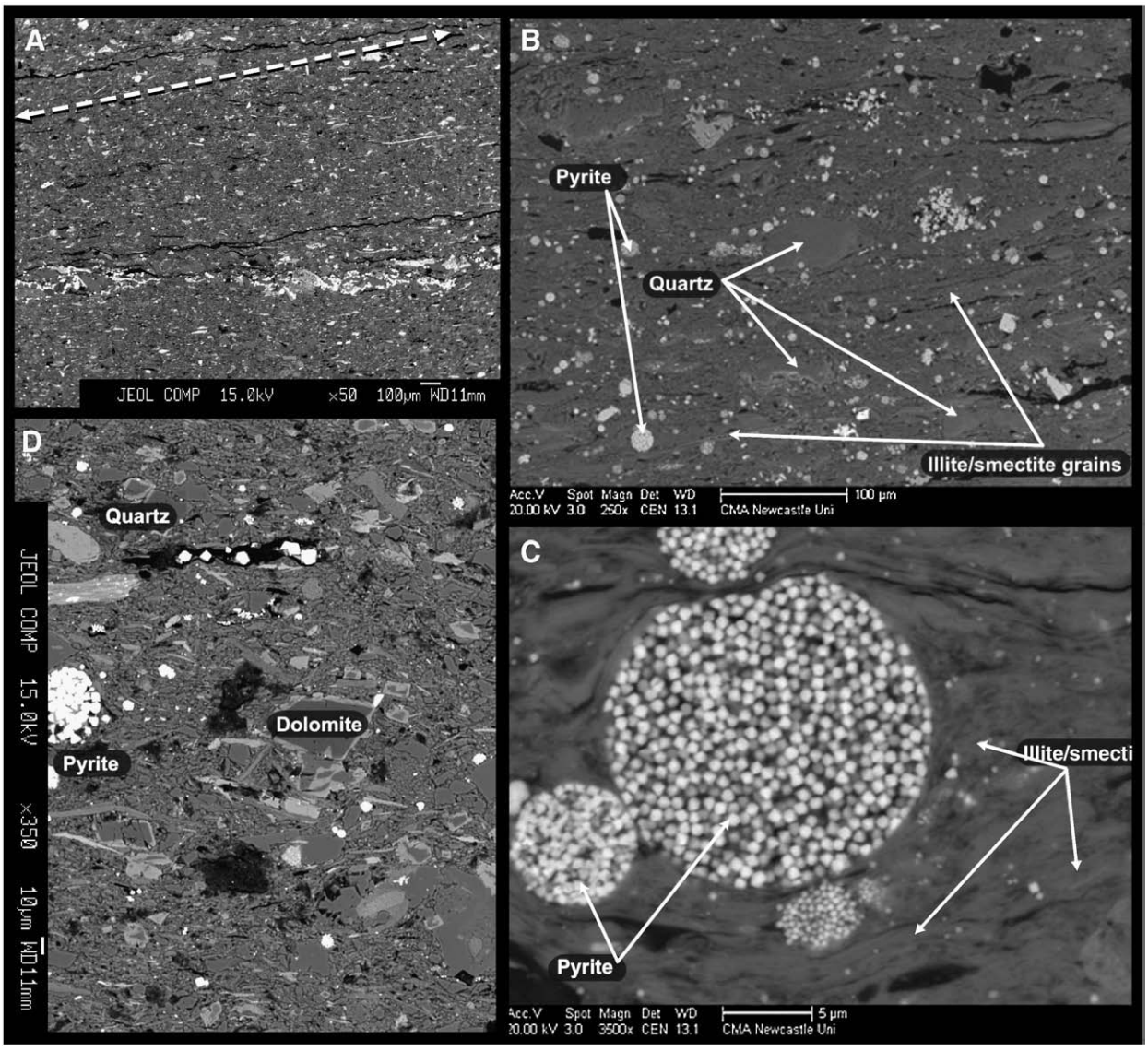


**Fig. 5.** BSE images. (A) Crews, (Cr08 5793 m) ×50 magnification quartz truncation of upwards fining unit, marked by dashed line. Bright backscatter contrast in quartz zone relates to Fe content in chlorite and ankerite. (B) Rhum, (4830.5 m) ×250 magnification. Fabric is orientated horizontally in the image, quartz and pyrite can be seen breaking up this alignment and the sample has parted along the line of the fabric in response to drying effects. The black areas on this image are organic material. (C) Rhum (4830.5 m) ×3500 magnification. Pyrite framboids with illite/smectite bending and wrapping around them. (D) Crews, (Cr20 5808 m) ×350 magnification. Fe-rims on dolomite, with pyrite framboids and little sorting of size fractions.

more illite in illite–smectite and most of the potassium feldspar in the system depleted. Given the percentage of illite in illite–smectite, we, therefore, interpret that the samples in this study have undergone complete reorientation of their phyllosilicates in response to diagenesis (Ho et al., 1999; Charpentier et al., 2003; Worden et al., 2005; Aplin et al., 2006; Day-Stirrat et al., 2008).

**Table 7**
Porosity and mean pore throat size distributions for samples from ARCO # W. L. Crews.

| Crews | Depth (m) | Temp °C | Porosity [%] | Mean pore throat size [nm] |
|---|---|---|---|---|
| cr-10 | 5795 | 187 | 9 | 10 |
| cr-17 | 5804 | 187 | 8 | 8 |
| cr-21 | 5809 | 187 | 7 | 8 |
| cr-26 | 6374 | 202 | 9 | 10 |
| cr-28 | 6376 | 202 | 8 | 13 |
| cr-29 | 6378 | 202 | 9 | 11 |
| cr-31 | 6603 | 210 | 10 | 13 |
| cr-36 | 6611 | 210 | 6 | 9 |
| cr-37 | 6612 | 210 | 9 | 10 |

Observations of BSE images (Figs. 3 and 5) suggest that fine-grained illite–smectite material is well aligned where quartz, dolomite and pyrite do not disrupt alignment. However, where equi-dimensional grains are present fabric is seen to be low. This may also be observed in the X-ray maps for potassium (Fig. 3), which we interpret to be predominantly a proxy for potassium-bearing clays (Table 1), either illite–smectite or mica. Optical light images (Fig. 4) do not allow mineralogical identification of clay-sized grains but do present a visual comparison of alignment and apparent upward fining.

Using the relationship between mudstone porosity and effective stress developed by Yang and Aplin (2004), Day-Stirrat et al. (2008) suggested that their shallowest samples (2.4 km burial, 55 wt.% clay content and 10% porosity) were at 27 MPa but were reluctant to calculate maximum effective stress for their deeper samples (6.6 km). Likewise, the samples from Rhum and Crews have low porosities commonly less than 10% (Table 7), and are deeply buried. The

estimated effective stress from Yang and Aplin (2004) applies only to mechanically compacted mudstones which may in reality be only applicable to the first 2–2.5 km of burial (Bjorlykke and Hoeg, 1997) after which diagenetic processes begin to control compaction and currently it is not possible to separate the effects of mechanical and non-mechanical diagenetic processes on porosity reduction.

The central question explored by the diagenetic reorientation model (Ho et al., 1999; Charpentier et al., 2003; Worden et al., 2005; Aplin et al., 2006; Day-Stirrat et al., 2008) is the extent to which mineralogical change drives reorientation of phyllosilicates in a burial setting. Each of these studies shows a relationship between the illitization of smectite and an increase in illite–smectite and kaolinite + chlorite fabric intensity. Day-Stirrat et al. (2008) document only a small increase in fabric intensity beyond the termination of the illitization of smectite in diagenetically well-constrained samples. This and previous studies assumes that initial depositional fabrics are composed of flocculated phyllosilicates that have an isotropic texture. Images by O'Brien (1971) show the often termed 'edge-to-face' and 'face-to-face' morphologies of these flocs immediately upon deposition. It is also implicit that floc deposition is controlled by floc size, the particle deposition model (Kranck and Milligan, 1985) that requires particle sizes to be greater than 10 μm. Within diagenetic reorientation studies a range of fabric intensities have been recorded from 1.88 m.r.d. (e.g. Aplin et al., 2006) (complete isotropy of 1.00 m.r.d. has never been recorded) to 6.99 m.r.d., the highest recorded illite–smectite fabric intensity from the Podhale Basin dataset (Day-Stirrat et al., 2008). Values for the Gulf Coast samples of Ho et al. (1999) are comparable. Fabric intensities in the range ~5.00–7.00 m.r.d. are rarely recorded at low temperatures/burial depths (50 °C). Therefore, what is controlling the range of phyllosilicate fabric intensities, 1.97–6.75 m.r.d., in the Rhum and Crews samples, given that there is ≤20% smectite in illite–smectite, temperatures greater than 150 °C, ≤10% porosity and high effective stress?

There is a positive relationship between whole-rock total clay content (Fig. 6) and illite–smectite fabric intensity and an inverse relationship between whole rock quartz content and illite–smectite fabric intensity. This supports the original data of Curtis et al. (1980), but extends the trend over a larger range of quartz contents (15–45 wt.%) and fabric intensity (~3.00–6.50 m.r.d.). When quartz contents increase beyond 45–50 wt.% in the whole rock, fabric intensities above 2.50–3.00 m.r.d. are not produced. Alternatively expressed, when total clay content in the whole rock is less than 45 wt.%, strong fabric intensities are not produced (Fig. 6). The key point about clay content is observable in the relationship between the 7 Å chlorite + kaolinite fabric intensity and these two mineral's contents in the whole rock. Samples having less than 3 wt.% of chlorite and kaolinite have a fabric intensity of ~2.00 m.r.d. or less. As fabric intensity increases close to the maximum diagenetically recorded values (e.g. Ho et al., 1999; Aplin et al., 2006; Day-Stirrat et al., 2008), there is a concomitant increase in chlorite and kaolinite content in the whole rock.

We may, therefore, make some predictions for post diagenetic fabric intensities based on the trends seen in Fig. 6. Samples from the Podhale Basin (Tables 1 and 2 in Day-Stirrat et al., 2008), at 5.7–7.0 km of maximum burial, have an illite–smectite fabric intensity ~6.00 m.r.d. and ~80% illite in illite–smectite. Using Fig. 6 this fabric intensity predicts 20–25 wt.% quartz and 55–60 wt.% total clay material. Published quantitative X-ray diffraction data (Srodon et al., 2006; Day-Stirrat et al., 2008) indicate that total clay content ranges from 51.2 to 55.5 wt.% for samples between 5.7 and 7.0 km of maximum burial and quartz content between 24.1 to 29.4 wt.%. This first-order agreement suggests there is predictive power in the relationships presented in Fig. 6. A prediction for the amount of quartz present in the 'sandy' samples of Ho et al. ((1999) see their Fig. 3) in the absence of quantitative X-ray diffraction data is possible. These samples are Cretaceous to late Tertiary in age and from the Texas Gulf Coast (Dewitt County) and have maximum burial depths of ~4.0 km. These samples have more than 80% illite in illite smectite yet the fabric

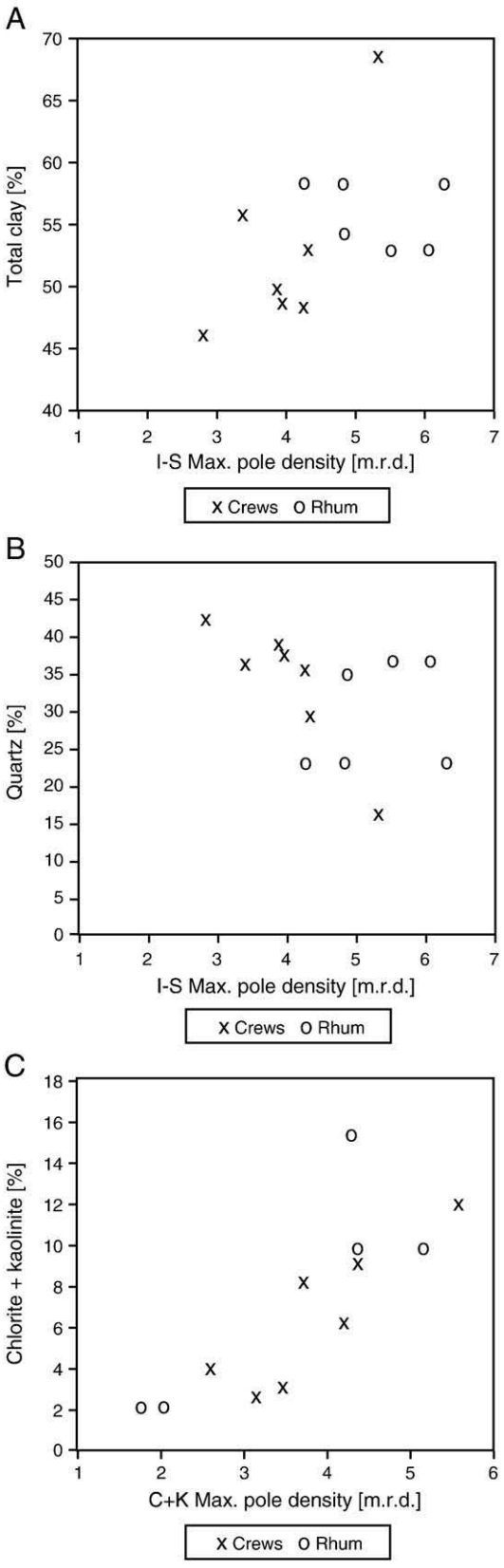


**Fig. 6.** (A) Relationship between I–S alignment (m.r.d.) and quartz [wt.%] in the Crews and Rhum wells. (B) Increasing alignment (m.r.d.) of chlorite and kaolinite with increasing chlorite and kaolinite content (wt.%) in the whole rock. (C) Relationship between I–S alignment (m.r.d.) and total clay [wt.%].

intensity is 3.34 to 3.58 m.r.d. We would predict ~40 wt.% quartz and ~45 wt.% total clay content. Two equations may be used to predict fabric intensity from (1) quartz content and (2) total clay content where:

$$y = -7.4x + 64.8 \quad (1)$$

$x$ is fabric intensity (in m.r.d.) and $y$ is total (wt.%) quartz

$$a = 4.2b + 33.7 \quad (2)$$

and $a$ is total (wt.%) clay content and b is fabric intensity (in m.r.d.).

Use of these equations is only applicable under certain conditions: (1) in the deep subsurface where bottom hole temperature higher than 140 °C, because clay minerals in most basins are diagenetically mature by this temperature; (2) fabric intensity is in the range of recorded values 1.80 to 7.00 m.r.d. Values lower than this are not always reliable, and higher are in the realm of metamorphism (Ho et al., 1995; Jacob et al., 2000) and subject to less well understood orientation processes. The potential for the kaolinite and chlorite phases measured at 7 Å to be treated in a similar predictive manner is lower. This is primarily due to concentration of these phases, which is generally much lower than illite–smectite (Tables 1 and 2 and data in Srodon et al., 2006). Lower concentrations can lead to a lack of correlation between the fabric intensities of illite–smectite and 7 Å kaolinite + chlorite noted for Rhum, deviating from the strong correlation noted in other studies (Day-Stirrat et al., 2008). The morphologies of kaolinite and chlorite are probably responsible for the lack of correlation with I–S in some samples. The 7 Å phase appears as an average of the fine-grained kaolinite that often decreases through burial diagenesis and large single chlorite grains, greater than 10 μm, that will not follow a floc deposition model and grow as neoformed phases perpendicular to effective stress (Day-Stirrat et al., 2008), making application of the 7 Å phase difficult.

The mechanism required in the diagenetic orientation model is one in which the illitization of smectite (Burst, 1959; Hower and Mowatt, 1966; Powers, 1967; Hower et al., 1976; Boles and Franks, 1979) proceeds through initial dissolution of a precursor phase and recrystallization into a neo-formed phase (Boles and Franks, 1979) or at least a partial dissolution (Ahn and Peacor, 1986; Inoue et al., 1987). The orientation of the precipitating phyllosilicates is governed by the direction of the principal effective stress; in a simple burial setting this is perpendicular to bedding. Silt-sized quartz grains, therefore, and any other equi-dimensional grain type that is significantly larger than the clay will disrupt the orientation of phyllosilicates in two ways: (1) phyllosilicates bend and wrap around non-platy surfaces; and (2) they shield the phyllosilicates from the vertical component of effective stress (Fig. 7). This is achieved either by sheltering the clays from compaction (see large scale "pressure shadows" caused by concretions in Lash and Blood, 2004) or by quartz grains acting as a rigid framework resulting in grain-to-grain contacts that are 'load-bearing', not allowing phyllosilicates to be influenced by effective stress, similar to an undeformed lithic clast in a sandstone. Quartz grain size is undoubtedly important to phyllosilicate reorientation but no systematic test has been completed as disaggregating well-lithified rocks does not produce meaningful data and image analysis on these fine-grained samples is cumbersome. Qualitatively, however, the effect of grain size can be seen in potassium X-ray maps (see Fig. 3) where quartz grains are large, and phyllosilicate alignment is poor. Also, the early diagenetic pyrite in the Kimmeridge Clay Formation (Fig. 5) exhibits some sheltering phenomena in which there is protection from the influence of effective stress (*sensu* "pressure shadow") and in Fig. 5 the coarser grains of the upper image do not show the lamination apparent in the lower. Like Curtis et al. (1980) we rule out bioturbation as a significant factor in governing fabric intensity in the deep subsurface. Appealing to the diagenetic

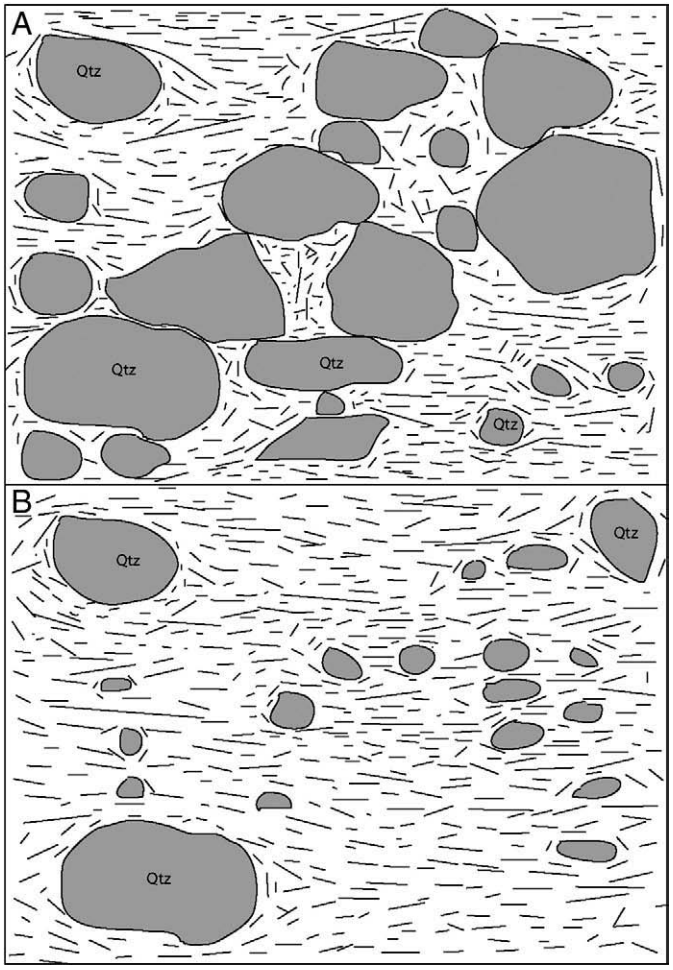


**Fig. 7.** (A) Silt size quartz grains in contact creating pressure shadows in which the overburden effective stress cannot 'see' the phyllosilicates. (B) Matrix supported quartz grains with isolated pressure shadows disrupting fabric, the majority of the phyllosilicates experience the vertical component of effective stress.

reorientation model we assume the ratio of platy phyllosilicates to equi-dimensional quartz at deposition to be the governing influence on the ability of the illitization of smectite to reorient phyllosilicate grains. The influence of bioturbation may be significant if it promotes quartz grain-to-grain contacts, but we see no evidence of this. Soft-sediment deformation, likewise, will have an effect on lamination rather than fabric in a post-diagenetic situation. This then leaves initial sediment water interactions (principally sorting) as the key control on post-diagenetic fabric intensity, where removal of the fine-fraction, on a millimeter scale, by scour in a fining-upwards (Bouma-like) sequence (Bouma, 1962; Stow and Shanmugan, 1980; Stow and Wetzel, 1990) may have an influence on unit anisotropy. When the upwards-fining sequence is truncated on a millimeter scale the fine-fraction of the sequence is lost and replaced by the coarser basal fraction of the overlying upwards fining unit. Therefore, the thickness of the fining-upwards unit can influence the mineralogical make-up of the system and its response to burial diagenesis, as well as its response to preferred clay mineral alignment. Seismic properties have been shown (Johnston and Christensen, 1995) to be strongly influenced by the alignment of phyllosilicates. Recorded anisotropies of shales with highly aligned phyllosilicates may have as much as 20% difference in the vertical and horizontal compressional and shear wave velocities in comparison to shallow buried non-aligned phyllosilicates that may be described as isotropic (Johnston and Christensen, 1995). The degree to which mudstones may have a preferred orientation of phyllosilicates in the deep subsurface is

dependent on initial composition and subsequent diagenesis. This composition control may impart an anisotropy in the response of these mudstones to wave propagation direction.

## 6. Conclusions

- In the units examined in this study there is an increase in illite–smectite preferred orientation with a decrease in whole-rock quartz content.
- High total clay contents in the whole rock result in increased illite–smectite alignments.
- There is a correlation between increasing kaolinite and chlorite contents in the whole rock XRPD data and an increase in the preferred orientation of the chloritechlorite + kaolinitekaolinite peak.
- Phyllosilicate alignment intensity is interpreted to be related to the thickness of upward-fining sequences on a millimeter scale in these samples, as scour has influenced the ratio of platy phyllosilicates to equi-dimensional quartz at deposition.
- Detrital quartz acts in two ways to disrupt phyllosilicate alignment: (1) phyllosilicates bend and wrap around silt sized particles and sit in spaces sheltered from compaction; and (2) act as load-bearing grains when in point contact that shields phyllosilicates between them from the influence of vertical effective stress.
- Two equations relating quartz and total clay contents to fabric intensity may be used as an empirical tool for expressing phyllosilicate anisotropy as a function of composition in the deep subsurface.

## Acknowledgments

James Iliffe of BP UK is thanked for help in facilitating sampling of the Rhum well. NERC are thanked for providing initial PhD funding to RJDS that allowed the Rhum 3/29a4 core to be analyzed. James Donnelly at the Austin Core Research Center (Bureau of Economic Geology University of Texas at Austin) is thanked for accessing the ARCO #1 W. L. Crews core. HRXTG is supported by EMAL at the University of Michigan and NSF grant EAR-0345985. We thank the John A. and Katherine G. Jackson School of Geosciences at the University of Texas at Austin and the member companies of the Bureau of Economic Geology Deep Shelf Gas Project for providing funding for this study.

Cathy Brown and Lana Dieterich are thanked for graphics and editing support. John Solum, an anonymous reviewer, and editor Gert Jan Weltje provided constructive reviews that improved this article. Published with permission of Director, Bureau of Economic Geology.

## References

Ahn, J.H., Peacor, D.R., 1986. Transmission and analytical electron microscopy of the smectite to illite transition. Clays and Clay Minerals 34, 165–179.
Angabini, A., 2003. Anisotropy of rock elasticity behavior and of gas migration in a Variscan Carboniferous rock mass in the South Limburg, The Netherlands. Engineering Geology 67, 353–372.
Aplin, A.C., Matenaar, I.F., McCarty, D.K., van der Pluijm, B.A., 2006. Influence of mechanical compaction and clay mineral diagenesis on the microfabric and pore-scale properties of deep-water Gulf of Mexico mudstones. Clays and Clay Minerals 54, 500–514.
Banik, N.C., 1984. Velocity anisotropy of shales and depth estimation in the North-Sea Basin. Geophysics 49, 1411–1419.
Bennett, R.H., O'Brien, N.R., Hulbert, H., 1991. Determinants of Clay and Shale Microfabric Signatures: Processes and Mechanisms. In: Bennett, R.H., Bryant, W.R., Hulbert, M.H. (Eds.), Microstructure of Fine-Grained Sediments. Springer Verlag.
Bjorlykke, K., Hoeg, K., 1997. Effects of burial diagenesis on stresses, compaction and fluid flow in sedimentary basins. Marine and Petroleum Geology 14, 267–276.
Boles, J.R., Franks, S.G., 1979. Clay diagenesis in Wilcox Sandstones of southwest Texas. Journal of Sedimentary Petrology 49, 55–70.
Bouma, A.H., 1962. Sedimentology of some flysch deposits. A graphic approach to facies interpretation. Elsevier, Amsterdam.
Burst, J.F., 1959. Postdiagenetic clay mineral environmental relationships in the Gulf Coast Eocene. Clays and Clay Minerals 6, 327–341.
Charpentier, D., Worden, R.H., Dillon, C.G., Aplin, A.C., 2003. Fabric development and the smectite to illite transition in Gulf of Mexico mudstones: an image analysis approach. Journal of Geochemical Exploration 78–79, 459–463.
Clavaud, J.B., Maineult, A., Zamora, M., Rasolofosaon, P., Schlitter, C., 2008. Permeability anisotropy and its relations with porous medium structure. Journal of Geophysical Research-Solid Earth 113.
Clennell, M.B., Dewhurst, D.N., Brown, K.M., Westbrook, G.K., 1999. Permeability anisotropy of consolidated clays. In: Aplin, A.C., Fleet, A.J., MacQuaker, J.H.S. (Eds.), Muds and Mudstones: Physical and Fluid Flow Properties: London. Special Publication, 158. Geological Society, London, pp. 79–96.
Corrigan, J., 2003, Correcting bottom hole temperature data, http://www.zetaware.com/utilities/bht/default.html.
Curtis, C.D., Lipshie, S.R., Oertel, G., Pearson, M.J., 1980. Clay orientation in some upper carboniferous mudrocks, its relationship to quartz content and some inferences about fissility, porosity and compactional history. Sedimentology 27, 333–339.
Day-Stirrat, R.J., Aplin, A.C., Srodon, J., van der Pluijm, B.A., 2008. Diagenetic reorientation of phyllosilicate minerals in Paleogene mudstones of the Podhale Basin, southern Poland. Clays and Clay Minerals 56, 100–111.
Delage, P., Lefebvre, G., 1984. Study of the structure of a sensitive champlain clay and of its evolution during consolidation. Canadian Geotechnical Journal 21, 21–35.
Dewhurst, D.N., Siggins, A.F., 2006. Impact of fabric, microcracks and stress field on shale anisotropy. Geophysical Journal International 165, 135–148.
Dutton, S.P., Loucks, R.G., 2010. Diagenetic controls on evolution of porosity and permeability in lower Tertiary Wilcox sandstones from shallow to ultradeep (200–6700 m) burial, Gulf of Mexico Basin, USA. Marine and Petroleum Geology 27 (1), 69–81.
Dutton, S.P., Loucks, R.G., 2008. Extending diagenetic trends in the Eocene Wilcox Formation with data from deep to ultradeep sandstones of the North Texas Gulf of Mexico Coast (abs.). AAPG 2008 Annual Convention and Exhibition Abstracts Volume 17, 50.
Fisher, R.S., McGowen, J.H., 1967. Depositional systems in the Wilcox Group of Texas and their relationship to occurrence of oil and gas. Gulf Coast Association of Geological Societies Transactions 17, 105–125.
Galloway, W.E., 2005. Gulf of Mexico basin depositional record of Cenozoic North American drainage basin evolution. Special Publication of the International Association of Sedimentologists. International, Blackwell, Oxford, International, pp. 409–423.
Galloway, W.E., McGilvery, T.A., 1995. Facies of a submarine canyon fill reservoir complex, lower Wilcox Group (Paleocene), central Texas Coastal Plain, SEPM Core Workshop, United States. Society of Economic Paleontologists and Mineralogists, United States, p. 1.
Galloway, W.E., Ganey-Curry, P.E., Li, X., Buffler, R., 2000. Cenozoic depositional history of the Gulf of Mexico basin. AAPG Bulletin 84, 1743–1774.
Glennie, K.W., 1998. Petroleum Geology of the North Sea: Basic concepts and recent advances. Blackwell Science, London.
Hillier, S., 1999. Use of an air brush to spray dry samples for X-ray powder diffraction. Clay Minerals 34, 127–135.
Hillier, S., 2002. Spray drying for X-ray powder diffraction preparation. IUCR Commission on Powder Diffraction Newsletter 27, 7–9.
Hillier, S., 2003. Quantitative analysis of clay and other minerals in sandstones by X-ray powder diffraction (XRPD). In: Worden, R.H., Morad, S. (Eds.), Clays and Clay cements in Sandstones. : International Association of Sedimentologists Special Publication, 34. Blackwell, Oxford, pp. 213–251.
Hillier, S., Matyas, J., Matter, A., Vasseur, G., 1995. Illite/smectite diagenesis and its variable correlation with vitrinite reflectance in the Pannonian basin. Clays and Clay Minerals 43, 174–183.
Ho, N.C., Peacor, D.R., van der Pluijm, B.A., 1995. Reorientation mechanisms of phyllosilicates in the mudstone-to-slate transition at Lehigh Gap, Pennsylvania. Journal of Structural Geology 17, 345–356.
Ho, N.C., Peacor, D.R., van der Pluijm, B.A., 1999. Preferred orientation of phyllosilicates in gulf coast mudstones and relation to the smectite–illite transition. Clays and Clay Minerals 47, 495–504.
Hoffman, J., Hower, J., 1979. Clay mineral assemblages as low grade metamorphic geothermometers: application to the trust faulted disturbed belt of Montana, U.S.A. In: Schole, P.A., Schluger, P.R. (Eds.), Society of Economic Paleontologists and Mineralogists: Special Publication, vol. 26, pp. 55–79.
Hower, J., Mowatt, T.C., 1966. The mineralogy of illites and mixed-layer illite–montmorillonites. American Mineralogist 51, 825–854.
Hower, J., Eslinger, E.V., Hower, M.E., Perry, E.A., 1976. Mechanism of burial metamorphism of argillaceous sediment 1. Mineralogical and chemical evidence. Geological Society of America Bulletin 87, 725–737.
Ibanez, W. D., A. K. Kronenberg, H. R. Wenk, and Anonymous, 1992, Anisotropy and the brittle-ductile deformation of shale AGU 1992 spring meeting v. 73, p. 309.
Inoue, A., Velde, B., Meunier, A., Touchard, G., 1987. Mechanism of illite formation during smectite-to-illite conversion in a hydrothermal system. American Mineralogist 73, 1325–1334.
Jacob, G., Kisch, H.J., van der Pluijm, B.A., 2000. The relationship of phyllosilicate orientation, X-ray diffraction intensity ratios, and c/b fissility ratios in metasedimentary rocks of the Helvetic zone of the Swiss Alps and the Caledonides of Jamtland, central western Sweden. Journal of Structural Geology 22, 245–258.
Jadgozinski, H., 1949. Eindimensionale Fehlordnung in Kristallen und ihr Einfluss auf die Röntgeninterferenzen. I. Berechnung des Fehlordnungsgrades aus den Röntgenintensitäten. Acta Crystallogr. Section A Foundations of Crystallography 2, 201–207.
Johansen, T.A., Jakobsen, M., Ruud, B.O., 2002. Estimation of the internal structure and anisotropy of shales from borehole data. Journal of Seismic Exploration 11, 363–381.
Johansen, T.A., Ruud, B.O., Jakobsen, M., 2004. Effect of grain scale alignment on seismic anisotropy and reflectivity of shales. Geophysical Prospecting 52, 133–149.

Johnston, J.E., Christensen, N.I., 1995. Seismic anisotropy of shales. Journal of Geophysical Research-Solid Earth 100, 5991–6003.
Kranck, K., Milligan, T.G., 1985. Origin of grain-size spectra of suspension deposited sediment. Geo-Marine Letters 5, 61–66.
Kranck, K., Smith, P.C., Milligan, T.G., 1996. Grain-size characteristics of fine-grained unflocculated sediments .1. 'One-round' distributions. Sedimentology 43, 589–596.
Kwon, O., Kronenberg, A.K., Gangi, A.F., Johnson, B., Herbert, B.E., 2004. Permeability of illite-bearing shale: 1. Anisotropy and effects of clay content and loading. Journal of Geophysical Research-Solid Earth 109, B10205.
Lash, G.G., Blood, D.R., 2004. Origin of shale fabric by mechanical compaction of flocculated clay: evidence from the Upper Devonian Rhinestreet Shale, western New York, USA. Journal of Sedimentary Research 74, 110–116.
MacQuaker, J.H.S., Curtis, C.D., Coleman, M.L., 1997. The role of iron in mudstone diagenesis: comparison of Kimmeridge clay formation mudstones from onshore and offshore (UKCS) localities. Journal of Sedimentary Research 67, 871–878.
Moore, D.M., Reynolds, R.C.J., 1997. X-ray Diffraction and the Identification and Analysis of Clay Minerals: Oxford. Oxford University Press, New York.
O'Brien, N.R., 1970. The fabric of shale—an electron microscope study. Sedimentology 15, 229–246.
O'Brien, N.R., 1971. Fabric of kaolinite and illite floccules. Clays and Clay Minerals 19, 353–359.
O'Brien, N.R., Slatt, R.M., 1990. Argillaceous Rock Atlas. Springer-Verlag, New York.
Oertel, G., Curtis, C.D., 1972. Clay-ironstone concretion preserving fabrics due to progressive compaction. Geological Society of America Bulletin 83, 2597–2605.
Okiongbo, K.S., 2005. Volumetrics of Petroleum Generation and Compaction of the Kimmeridge Clay Formation. Unpublished PhD Thesis Thesis, University of Newcastle-Upon-Tyne.
Omotoso, O., McCarty, D.K., Hillier, S., Kleeberg, R., 2006. Some successful approaches to quantitative mineral analysis as revealed by the 3rd Reynolds Cup contest. Clays and Clay Minerals 54, 748–760.
Powers, M.C., 1967. Fluid-release mechanisms in compacting marine mudrocks and their importance in oil exploration. American Association of Petroleum Geologists Bulletin 51, 1240–1254.
Pytte, A.M., Reynolds Jr., R.C., 1989. The kinetics of the smectite to illite reaction in contact metamorphic shales. In: Naeser, N.D., McCulloch, T.H. (Eds.), The Thermal History of Sedimentary Basins. Springer-Verlag, New York, pp. 133–140.
Sayers, C.M., 1999. Stress-dependent seismic anisotropy of shales. Geophysics 64, 93–98.
Sayers, C.M., 2005. Seismic anisotropy of shales. Geophysical Prospecting 53, 667–676.
Schon, J.H., Georgi, D.T., Tang, X.M., 2006. Elastic wave anisotropy and shale distribution. Petrophysics 47, 239–249.
Sintubin, M., 1994. Clay fabrics in relation to the burial history of shales. Sedimentology 41, 1161–1169.
Sintubin, M., 1995. High-resolution X-ray texture goniometry: discussion. Journal of Structural Geology 17, 923–924.
Srodon, J., Kotarba, M., Biron, A., Such, P., Clauer, N., Wojtowicz, A., 2006. Diagenetic history of the Podhale–Orava Basin and the underlying Tatra sedimentary structural units (Western Carpathians): evidence from XRD and K–Ar of illite–smectite. Clay Minerals 41, 751–774.
Stow, D.A.V., Shanmugan, G., 1980. Sequences structures in fine-grained turbidities; comparison of recent deep-sea and ancient flysch sediments. Sedimentary Geology 25, 23–42.
Stow, D.A.V., Wetzel, A., 1990. Hemiturbidite:a new type of deep-water sediment. In: Cochan, J.R., Stow, D.A.V. (Eds.), Proceedings of the ODP scientific results, vol. 116, pp. 25–34.
Valcke, S.L.A., Casey, M., Lloyd, G.E., Kendall, J.M., Fisher, Q.J., 2006. Lattice preferred orientation and seismic anisotropy in sedimentary rocks. Geophysical Journal International 166, 652–666.
van der Pluijm, B.A., Ho, N.-C., Peacor, D.R., 1994. High-resolution X-ray texture goniometry. Journal of Structural Geology 16, 1029–1032.
van der Pluijm, B.A., Ho, N.-C., Peacor, D.R., 1995. High-resolution X-ray texture goniometry: Reply. Journal of Structural Geology 17, 925–926.
Van Rensbergen, P., Morley, C.K., 2003. Re-evaluation of mobile shale occurrences on seismic sections of the Champion and Baram Deltas, offshore Brunei. Geological Society Special Publications. Geological Society of London, London, pp. 395–409.
Vernik, L., Landis, C., 1996. Elastic anisotropy of source rocks: Implications for hydrocarbon generation and primary migration. Aapg Bulletin-American Association of Petroleum Geologists 80, 531–544.
Walker, J.R., 1993. Chlorite polytype geothermometry. Clays and Clay Minerals 41, 260–267.
Wenk, H.R., 1985. Measurement of pole figures. In: Wenk, H.R. (Ed.), Preferred orientation in deformed metals and rocks: An introduction to modern texture analysis. Academic Press, INC, pp. 11–48.
Worden, R.H., Charpentier, D., Fisher, Q.J., Aplin, A.C., 2005. Fabric development and the smectite to illite transition in Upper Cretaceous mudstones from the North Sea: an image analysis approach. In: Shaw, R.P. (Ed.), Understanding the Micro to Macro Behaviour of Rock-Fluid Systems. : Special Publications, vol. 249. Geological Society, London, pp. 103–114.
Yang, Y.L., Aplin, A.C., 2004. Definition and practical application of mudstone porosity-effective stress relationships. Petroleum Geoscience 10, 153–162.